

See discussions, stats, and author profiles for this publication at: <https://www.researchgate.net/publication/282049753>

# Thermal Fluctuations on Förster Resonance Energy Transfer in Dyadic Solar Cell Sensitizers: A Combined Ab Initio Molecular Dynamics and TDDFT Investigation

ARTICLE *in* THE JOURNAL OF PHYSICAL CHEMISTRY C · JULY 2015

Impact Factor: 4.77 · DOI: 10.1021/acs.jpcc.5b04921

---

READS

77

## 6 AUTHORS, INCLUDING:



Sergio Rampino

Consiglio Nazionale delle Ricerche, Italy

32 PUBLICATIONS 134 CITATIONS

[SEE PROFILE](#)



Ramiro Arratia-Perez

Universidad Andrés Bello

149 PUBLICATIONS 1,220 CITATIONS

[SEE PROFILE](#)



Mariachiara Pastore

Italian National Research Council

52 PUBLICATIONS 1,252 CITATIONS

[SEE PROFILE](#)



Filippo De Angelis

Università degli Studi di Perugia

266 PUBLICATIONS 11,245 CITATIONS

[SEE PROFILE](#)

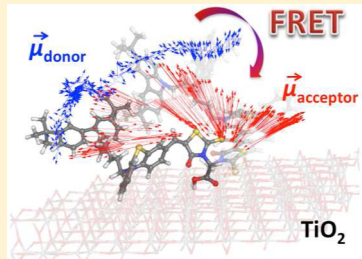
# Thermal Fluctuations on Förster Resonance Energy Transfer in Dyadic Solar Cell Sensitizers: A Combined Ab Initio Molecular Dynamics and TDDFT Investigation

Rodrigo A. Urzúa-Leiva,<sup>†,‡</sup> Sergio Rampino,<sup>\*,†</sup> Ramiro Arratia-Perez,<sup>‡</sup> Edoardo Mosconi,<sup>†</sup> Mariachiara Pastore,<sup>\*,†</sup> and Filippo De Angelis<sup>\*,†</sup>

<sup>†</sup>Computational Laboratory for Hybrid/Organic Photovoltaics (CLHYO), CNR-ISTM, Via Elce di Sotto 8, 06123 Perugia, Italy

<sup>‡</sup>Relativistic Molecular Physics (ReMoPh) Group, Ph.D. Program in Molecular Physical Chemistry, Universidad Andrés Bello, Av. República 275, Santiago 8370146, Chile

**ABSTRACT:** Förster resonance energy transfer (FRET) is a key process in dyadic dye-sensitized solar cells (DSSCs) where an “antenna” donor has the role of collecting photons and redirecting the captured energy to an adsorbed-dye acceptor unit. Despite its popularity in, e.g., biology, where FRET rates are used to derive structural information on fairly complex systems, relatively few studies have appeared in the DSSCs field. These were based, to the best of our knowledge, either on a static modeling of FRET or on the so-called isotropic regime assuming an isotropic motion of the donor/acceptor units and uncorrelated donor/acceptor relative distance and orientation. In this paper we carry out a combined Car–Parrinello molecular dynamics and TDDFT investigation to unravel the impact of thermal fluctuations on FRET in two dyadic carbazole–phenothiazine dye sensitizers. Both isolated and full-packed adsorption conditions are considered, mimicking the dye adsorption topology on TiO<sub>2</sub>. Results are discussed in relation to the above mentioned models and rationalized in terms of the structural differences of the considered dyes. We find a considerable difference between the FRET rates calculated at zero temperature and the results obtained by including thermal fluctuations, highlighting an important role of the latter in determining FRET rates in dyadic donor–acceptor dye-sensitized solar cells.



## 1. INTRODUCTION

Up to the “perovskite” revolution in 2012,<sup>1,2</sup> dye-sensitized solar cells (DSSCs)<sup>3–5</sup> have represented the leading alternative technology to traditional silicon-based devices, with top certified efficiency exceeding 11% and laboratory-cell efficiency above 13%.<sup>6</sup> Although the highest-performance devices employing liquid I<sup>−</sup>/I<sub>3</sub><sup>−</sup> electrolyte<sup>7</sup> are sensitized with Ru(II)-based dyes,<sup>8–11</sup> a variety of metal-free dyes were developed,<sup>12–14</sup> with overall efficiencies reaching 13% when a cobalt-based electrolyte is employed.<sup>6,15–20</sup> Panchromatic sensitization of the electron transporting semiconductor, generally TiO<sub>2</sub>, is achieved in this case either by optimizing the optical and structural properties of individual dyes or by mixing different sensitizers (“co-sensitization”) having complementary absorption spectra.<sup>21–27</sup> Co-sensitization presents however two main drawbacks: (i) restrictions due to a limited TiO<sub>2</sub> loading and (ii) difficulties in controlling and optimizing the coadsorption geometry to increase the light collection efficiency and suppress parasitic deactivation pathways. Alternatively, a widely employed molecular engineering approach to increase the dye efficiency by extending the portion of absorbed light consists in loading dyes with tethered “antenna” systems,<sup>28–33</sup> the latter having the role of collecting photons and redirecting the captured energy via long-range energy transfer (so-called Förster or fluorescence-detected resonance energy transfer,

hereafter FRET)<sup>34</sup> to the sensitizing dye, which is adsorbed onto the semiconductor surface.<sup>35</sup>

FRET is a nonradiative energy transfer process from the excited-state of an electron “donor” (D) to the excited-state of an electron “acceptor” (A). FRET processes are mediated by dipole–dipole interactions, where the energy transfer efficiency is mainly determined by the distance and geometrical orientation between the donor and acceptor moieties in the combined system.<sup>36</sup> On these grounds, FRET has been extensively used to obtain structural information about complex biological systems (i.e., position and orientations of donor and acceptor fluorophores)<sup>37,38</sup> in experiments based on a large variety of fluorescence methodologies.<sup>39–42</sup> Despite such popularity in deriving quantitative structural information on biological macromolecules, the validity of the fundamental assumptions underlying the modeling of FRET processes has recently been questioned.<sup>43–48</sup> Basically, the most debated issue is the so-called “isotropic regime”, whereby both the donor and the acceptor are assumed to rapidly sample all possible orientations, resulting in an average orientational factor for the dipolar interaction ( $\kappa^2$ , *vide infra*) of 2/3. A second assumption which is implied in the isotropic model is that the

Received: May 22, 2015

Revised: June 26, 2015

Published: June 26, 2015

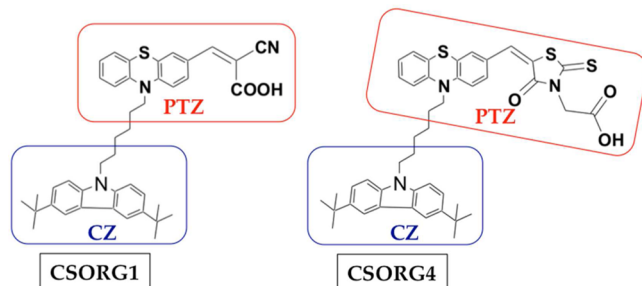


distance between the donor and the acceptor unit is not correlated to their relative orientations.<sup>47</sup> As a consequence, in recent years, molecular dynamics (MD) simulations have been largely employed to study the simultaneous motion of the donor/acceptor pair, thus supporting FRET experiments in obtaining structural parameters in various fields, including biology.<sup>48,49–53</sup>

As already mentioned, FRET has been utilized in DSSCs technologies to extend the light-harvesting capability of the dye-sensitized TiO<sub>2</sub> photoanode. As a matter of fact, however, relatively few computational investigations have appeared so far and, to the best of our knowledge, only limited to a static picture of the process.<sup>54–57</sup> If inclusion of dynamical aspects is expected to have a relatively small impact when the FRET process occurs between coadsorbed donor and acceptor units in close packing,<sup>55</sup> it becomes, in principle, mandatory in dyadic systems. Here, in fact, thermal fluctuations might strongly influence the FRET parameters due to the high flexibility of the linker chain connecting the “antenna” moiety (donor) with the sensitizing dye (acceptor).

In this paper, we tackle the dynamical modeling of FRET processes in dyadic dye sensitizers combining Car-Parrinello molecular dynamics (CPMD) and time dependent DFT simulations. We consider two dyadic carbazole–phenothiazine (CZ-PTZ) dyes recently characterized by some of us<sup>56</sup> where the CZ unit, linked to PTZ via an alkyl C<sub>6</sub>H<sub>12</sub> chain, acts as an antenna donor and the PTZ unit is a TiO<sub>2</sub>-anchored acceptor. The two dyes (see Scheme 1), hereafter termed CSORG1 and

**Scheme 1.** Molecular Structures of the CSORG1 and CSORG4 Dyes<sup>a</sup>



<sup>a</sup>Donor (CZ) and acceptor (PTZ) moieties are enclosed in blue and red frames, respectively.

CSORG4 after ref 56, differ for the anchoring group and hence for the relative mobility of the CZ and PTZ constituents. CSORG1 shows electron conjugation between PTZ and the cyanoacrylic acid anchoring group, enforcing the PTZ moiety to an almost perpendicular arrangement with respect to the TiO<sub>2</sub> surface. In CSORG4, on the contrary, the PTZ moiety is allowed to bend more freely about the rhodanine-3-acetic acid anchoring group.

We monitor the dynamical evolution of the FRET geometrical parameters along the CPMD trajectories for the two dyes mimicking both the isolated and full-packed TiO<sub>2</sub> adsorption conditions, accounting for both intramolecular and intermolecular energy transfers. The results are discussed in relation to the assumptions underlying the above-mentioned models, showing a sizable difference between the static and dynamical FRET picture. This finding is in line with the conclusions of very recent studies highlighting the importance

of including thermal fluctuations in the calculations of interchromophoric coupling in organic crystals.<sup>58–60</sup>

The paper is organized as follows. In section 2, models and computational details are discussed. In section 3, results are presented. We first analyze the time-evolution of the geometrical parameters (the donor/acceptor relative distance and orientation) concurring in determining FRET (section 3.1), then address the correlation between them (section 3.2), and finally carry out a comparison of the FRET-rate estimates in the static, isotropic, and dynamical model (section 3.3). Conclusions are drawn in section 4.

## 2. MODELS AND COMPUTATIONAL DETAILS

**2.1. Modeling FRET.** According to the popular formulation by Förster,<sup>61</sup> the FRET rate is given by

$$k_F = \frac{1R_0^6}{\tau_0 r_{DA}^6} \quad (1)$$

where  $\tau_0$  is the lifetime of the donor excited state,  $R_0$  is the so-called Förster radius, and  $r_{DA}$  is the donor–acceptor distance, usually taken as the distance between the center of the nuclear charges of CZ and that of PTZ.<sup>56</sup> The Förster radius, can be obtained from the donor luminescence efficiency,  $Q_D$ , the overlap integral of the donor emission spectrum,  $F_D$ , and the acceptor absorption spectrum  $\varepsilon_A$ , and the orientation factor  $\kappa^2$ :

$$R_0^6 = \frac{9000 \times \ln(10)\kappa^2 Q_D}{128\pi^5 n^4 N_A} \int F_D(\lambda) \varepsilon_A(\lambda) \lambda^4 \, d\lambda \quad (2)$$

with  $N_A$  being the Avogadro's number and  $n$  the refractive index of the medium. The dimensionless orientation factor  $\kappa^2$  ranges from 0 to 4 and is given by

$$\kappa^2 = (\cos \gamma - 3 \cos \alpha \cos \beta)^2 \quad (3)$$

where the angles  $\alpha$ ,  $\beta$ , and  $\gamma$  define the relative orientation between the two interacting dipole moments (high  $\kappa^2$  values relate to parallel relative orientation favoring FRET; low values to perpendicular relative orientation; see ref 36 for details).

It is common practice to assume all photophysical quantities in eqs 1 and 2 ( $\tau_0$ ,  $Q_D$  and the overlap integral between the donor emission and the acceptor absorption spectra) to be independent of the dynamical structural changes.<sup>47</sup> The FRET rate eq 1 can, therefore, be put in the form

$$k_F = C \kappa^2 r_{DA}^{-6} = C k'_F \quad (4)$$

where we have introduced the scaled FRET rate  $k'_F$  having units of Å<sup>-6</sup>.

**2.2. Model Structures.** A schematic representation of the (101) anatase TiO<sub>2</sub> surface, representing the majority surface exposed in mesoporous TiO<sub>2</sub> films, is given in Figure 1. The primitive cell has dimensions  $a_0 = 3.78$  Å and  $b_0 = 10.24$  Å. As mentioned in the Introduction, CSORG1 and CSORG4 feature different anchoring groups inducing a markedly different adsorption minimum-energy configuration onto the semiconductor surface.<sup>62</sup> CSORG1, in fact, due to conjugation between PTZ and the anchoring group, stands up almost perpendicular to the TiO<sub>2</sub> surface while CSORG4, showing not such conjugation, lies bent over the surface plane. Accordingly, the minimal area to accommodate one anchored molecule of CSORG4 (right panel of Figure 1) without atomic superimpositions with periodic images ( $4a_0 \times 2b_0$  dashed blue

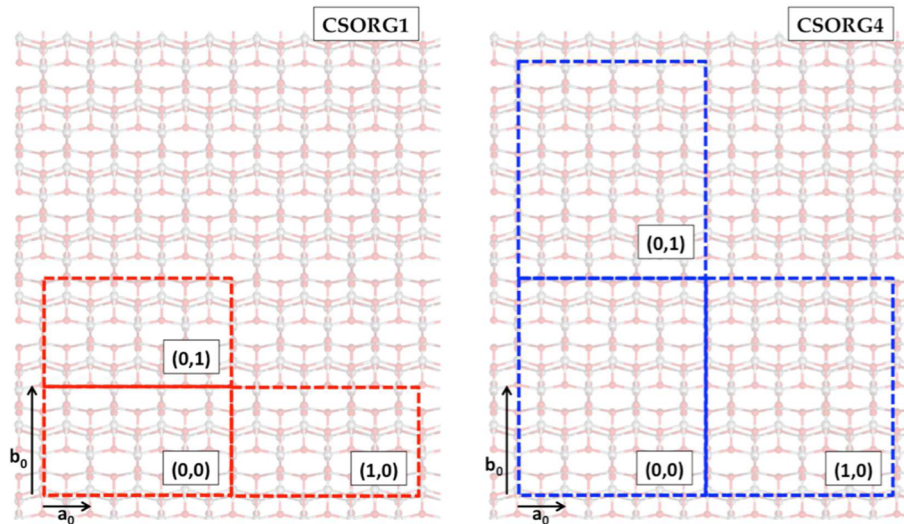


**Figure 1.** Scheme of the penta-coordinated Ti atoms in the anatase  $\text{TiO}_2$  (101) surface, representing the grid of possible dye adsorption sites. The supercells employed for full-packed CSORG1 (left panel) and CSORG4 (right panel) are demarcated as dashed red frames and dashed blue frames, respectively, corresponding each to the minimal surface area for full coverage by the dye. Neighbor supercells to a reference cell (0,0) along the  $a$  and  $b$  directions are termed (1,0) and (0,1), respectively.

frames) is twice that required by CSORG1 ( $4a_0 \times 1b_0$  dashed red frames in the left panel).

In the considered framework, the isolated dyes are simulated by employing large supercells to decouple the electronic and steric influence of the neighboring dyes in the periodic replica. By reducing the dimensions of the simulated supercells to the minimum dimension preserving the  $\text{TiO}_2$  periodicity and avoiding atomic superimpositions, we basically reduce the space between periodically replicated dye images, thus effectively sampling intermolecular interactions. For simulations of the isolated dyes, an orthorhombic supercell of  $32 \times 32 \times 32 \text{ \AA}^3$  was employed, within periodic boundary conditions. For full-packed simulations smaller supercells of  $4a_0 \times 1b_0 \times 32$  (i.e.,  $15.16 \times 10.24 \times 32 \text{ \AA}^3$  and  $4a_0 \times 2b_0 \times 32$  (i.e.,  $15.16 \times 20.48 \times 32 \text{ \AA}^3$  for CSORG1 and CSORG4, respectively, were used. The interaction with the  $\text{TiO}_2$  surface is not explicitly taken into account, and the bidentate adsorption mode<sup>56</sup> is enforced by fixing the atomic coordinates of the carboxylate anchoring moiety to those obtained in the optimized dye/ $\text{TiO}_2$  assemblies.<sup>56</sup>

**2.3. Computing FRET Parameters.** The FRET geometrical parameters (donor–acceptor distance  $r_{\text{DA}}$  and the dipole-orientation factor  $\kappa^2$  entering eq 4) were computed for a set of 474 snapshots along the CPMD trajectories (see next Section for CPMD details). At each snapshot, the structures of the donor (CZ) and acceptor (PTZ) moieties of both CSORG1 and CSORG4 were extracted from the respective entire-dye structure by cutting the alkyl chain departing from the selected (CZ or PTZ) unit after two carbon atoms (see Scheme 1) and saturating with H ( $-\text{C}_2\text{H}_5$ ). The donor–acceptor distance  $r_{\text{DA}}$  was taken to be the distance between the center of the nuclear charges of CZ and that of PTZ. Transition dipole moments for the first and brightest excited state were calculated by TDDFT with the Gaussian 09 program package,<sup>63</sup> using the hybrid MPW1K xc functional<sup>64</sup> and a 6-31G\* basis set. Solvent (THF) effects were included by the conductor-like polarizable continuum model (C-PCM).<sup>65</sup> A check was run ensuring that including more than two  $-\text{CH}_2-$  units in the

definition of the CZ and PTZ units left unchanged the transition dipole moment components.

To model the probability of intermolecular CZ  $\rightarrow$  PTZ FRET in an ideally full-covered  $\text{TiO}_2$  surface one has to deal with all possible combinations of donor–acceptor couples along both  $a$  and  $b$  directions of Figure 1. Considering the dye in a reference cell hereafter termed (0,0) (see Figure 1), in full-packed conditions the first neighbor molecule along  $b$  will be placed in a top-adjacent cell, that we indicate as (0,1), while that along  $a$  in a right-adjacent cell, that we indicate as (1,0). According to this scheme, the following donor–acceptor couples can be defined:

- CZ(0,0)  $\rightarrow$  PTZ(0,0) (intramolecular)
- CZ (0,0)  $\rightarrow$  PTZ (1,0) (intermolecular)
- CZ (1,0)  $\rightarrow$  PTZ (0,0) (intermolecular)
- CZ (0,0)  $\rightarrow$  PTZ (0,1) (intermolecular)
- CZ (0,1)  $\rightarrow$  PTZ (0,0) (intermolecular)

Since we expect the intramolecular FRET to be the predominant energy transfer channel in this kind of system and just aim at having a rough estimate of the possible intermolecular components, we calculate the intermolecular FRET parameters by translating along the  $a$  and  $b$  directions the CZ and PTZ nuclear charge centers and transition dipole moments obtained from the single dye molecule under full-packed conditions. This approximation was beforehand validated on a set of six representative CPMD snapshots by comparing the CZ and PTZ transition dipole moments of a the dye in full-packed conditions with those obtained in a two-dye calculations explicitly accounting for the presence of the adjacent (both (1,0) and (0,1)) cell. We find only negligible differences and an overall comparable trend as a function of the simulation time.

**2.4. Car–Parrinello Molecular Dynamics.** To simulate the effect of thermal fluctuations in FRET we calculated the dimensionless factor  $\kappa^2$ , the donor–acceptor separation,  $r_{\text{DA}}$ , and the scaled energy transfer rate,  $k'_F = k_F/C$  (see eq 4), for the selected CPMD snapshots, extracted at steps of 42.3 fs along the differently calculated trajectories of the isolated and full-packed CSORG1 and CSORG4 systems. The geometries of

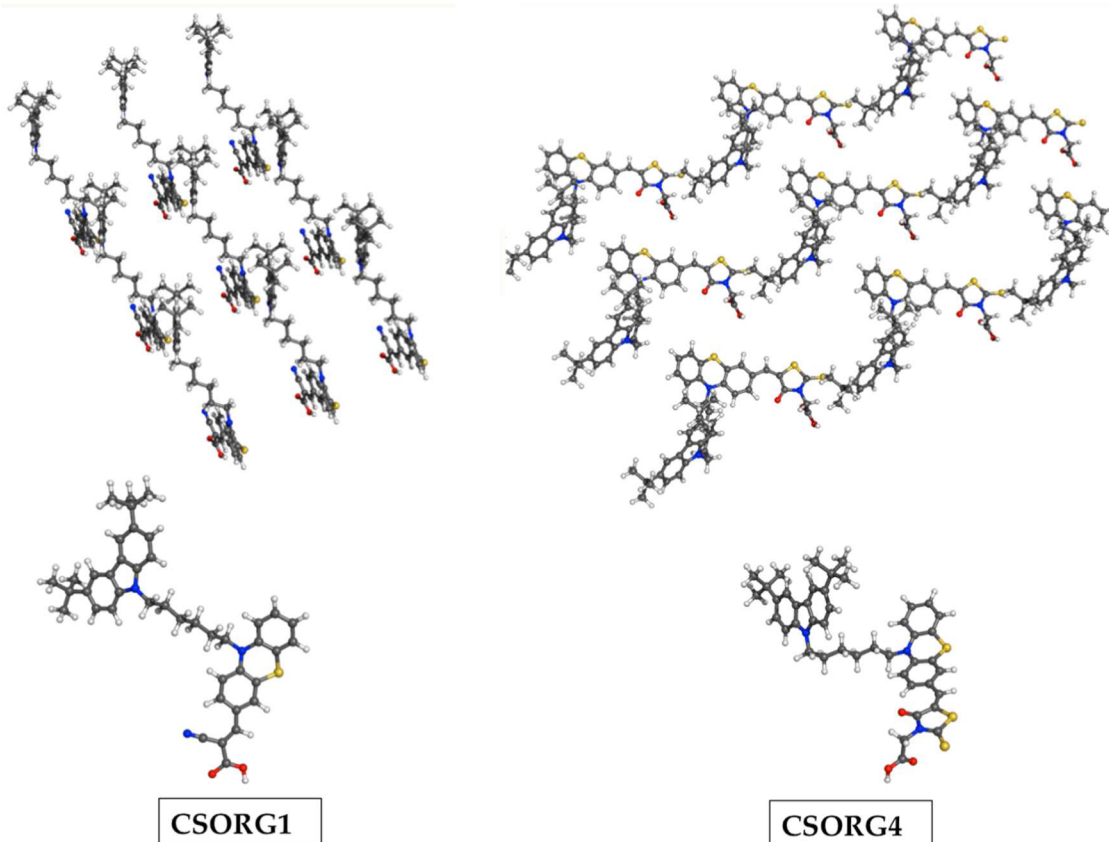


**Figure 2.** Optimized molecular structure of the full-packed (top) and isolated (bottom) CSORG1 (left) and CSORG4 (right) dyes.

CSORG1 and CSORG4 were preliminarily optimized at CP level of theory in both isolated and full-packed conditions. CPMD simulations<sup>66</sup> were carried out with the Quantum-Espresso package,<sup>67</sup> employing the BLYP exchange-correlation functional<sup>68,69</sup> in combination with a plane wave basis set and ultrasoft pseudopotentials.<sup>70</sup> Plane wave basis set cutoffs set for the smooth part of the wave functions and the augmented density are 25 and 200 Ry, respectively. The Brillouin zone is sampled using the gamma-point only. The fictitious electron mass in the CP lagrangian was set to 500 au and the atom masses to the real masses except for the H atoms for which we set a mass value of 2 au. An integration time step of 5 a.u. was used, simulating the systems for a total of ca. 20 ps. Considering this simulation time, the slowest sampled modes fall in the far IR region where molecular-skeleton vibrations and molecular torsions occur. This should be sufficient to account for the thermal fluctuations affecting the FRET parameters in the full-coverage working conditions effectively employed in DSSC devices. A temperature of  $300 \pm 25$  K was set using the Nosé–Hoover thermostat. This set up allows us to effectively perform the nuclear thermalization and to maintain the adiabaticity throughout the simulation.

### 3. RESULTS AND DISCUSSION

**3.1. FRET Geometrical Parameters.** The optimized geometries of CSORG1 and CSORG4 in both isolated and full-packed adsorption conditions do not differ substantially, as is apparent in Figure 2. Notice the upright configuration of CSORG1 versus the leaning one of CSORG4 due to the presence/absence, respectively, of conjugation between the PTZ unit and the anchoring group. The calculated CZ-PTZ

distance  $r_{\text{DA}}$  and orientation factor  $\kappa^2$  values corresponding to this static, CP-optimized picture are reported in Table 1. As is apparent, the presence in CSORG4 of a nonconjugated rhodanine-anchoring group inducing a leaning orientation of the donor PTZ moiety with respect to the surface plane yields a shorter CZ-PTZ distance (10.98 Å) when compared to that of

**Table 1.** Static (CP-Optimized), Average, Minimum, and Maximum Values of the FRET Geometrical Parameters ( $r_{\text{DA}}$  and  $\kappa^2$ ) for CSORG1 and CSORG4 along the CPMD Simulation under both Isolated and Full-Packed Conditions<sup>a</sup>

	static	average	min. (time of min.)	max. (time of max.)
CSORG1				
isolated				
$r_{\text{DA}}$ (Å)	12.36	11.42	8.17 (16.85 ps)	13.64 (11.35 ps)
$\kappa^2$	0.58	0.99	0.00 (1.74 ps)	3.59 (12.28 ps)
full-packed				
$r_{\text{DA}}$ (Å)	12.32	11.70	8.86 (19.26 ps)	13.13 (4.49 ps)
$\kappa^2$	0.51	1.08	0.00 (7.87 ps)	3.47 (10.24 ps)
CSORG4				
isolated				
$r_{\text{DA}}$ (Å)	10.98	11.41	7.27 (13.55 ps)	13.63 (8.59 ps)
$\kappa^2$	0.24	0.82	0.00 (1.82 ps)	2.99 (17.44 ps)
full-packed				
$r_{\text{DA}}$ (Å)	11.29	11.17	6.63 (14.99 ps)	13.80 (6.35 ps)
$\kappa^2$	0.31	0.99	0.00 (5.59 ps)	3.56 (19.35 ps)

<sup>a</sup>The simulation time when minimum and maximum values are recorded are also given.

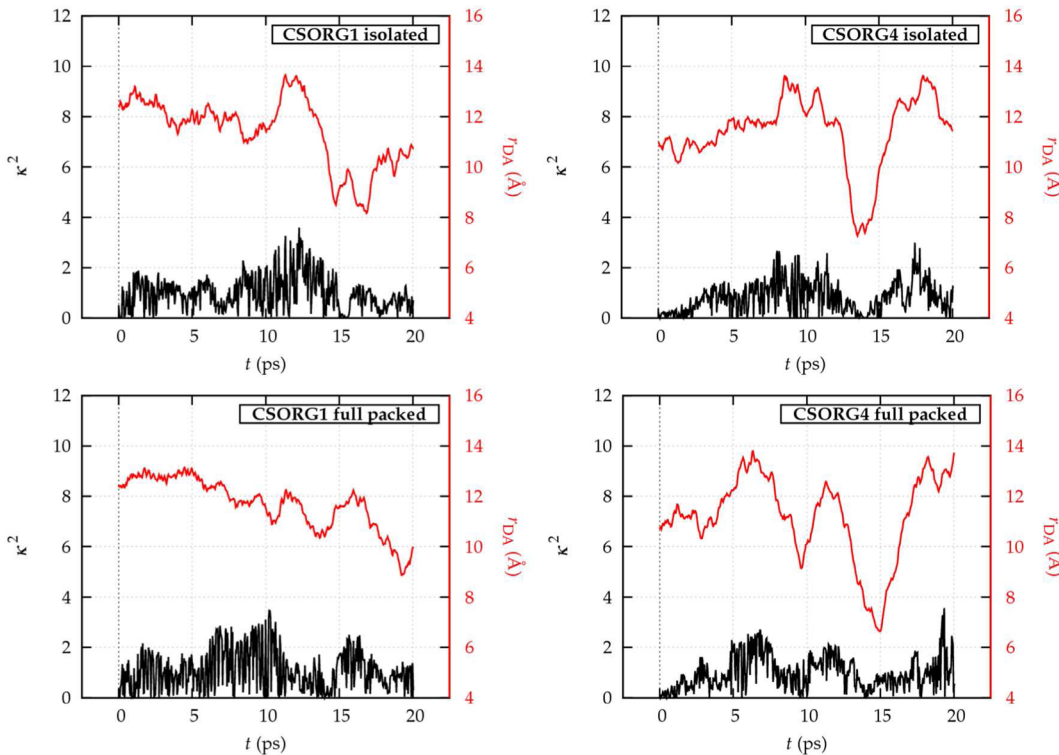


**Figure 3.** Donor–acceptor distance  $r_{\text{DA}}$  (red line, right-hand-side scale) and orientation factor  $\kappa^2$  (black line, left-hand-side scale) as a function of the CPMD simulation time for both CSORG1 (left panels) and CSORG4 (right panels) under isolated (top panels) and full-packed conditions (bottom panels).

the upright standing CSORG1 (12.36 Å). The relative orientation between the transition dipole moments, however, seems to favor CSORG1 compared to CSORG4, with a  $\kappa^2$  of 0.58 and 0.24 for the CSORG1 and CSORG4, respectively.

In Figure 3, the instantaneous values of  $r_{\text{DA}}$  and  $\kappa^2$  for CSORG1 (left panels) and CSORG4 (right panels) obtained from the CPMD simulations in isolated (top panels) and full-packed (bottom panel) conditions are plotted as a function of time. Average, minimum and maximum values are listed in Table 1, along with the simulation time when minimum and maximum values are recorded.

Focusing on the isolated CSORG1, the donor–acceptor distance is seen to remain almost constant during the first half (about 10 ps) of the simulation, showing a maximum (13.64 Å) at 11.35 ps and then slight decreasing in the last simulation slice. The minimum distance, 8.17 Å, is registered at 16.85 ps. As is apparent, full coverage appreciably affects the CZ-PTZ separation, which in full-packed conditions shows its maximum value (13.13 Å) within the first 5 ps of the simulation (4.49 ps), then slowly decreases undergoing large oscillations until reaching its minimum value (8.86 Å) after 19.26 ps of simulation. As to the orientation factor  $\kappa^2$ , interestingly, whereas its maximum recorded value in isolated and full-packed conditions almost coincides (3.59 vs 3.47 respectively), the trend observed along the trajectories is rather different. In fact, close-packing seems to induce ampler fluctuations in the relative orientation of CZ and PTZ than those observed for isolated CSORG1, and, on average, a greater  $\kappa^2$  (1.08 to be compared with 0.99). We note that both these average  $\kappa^2$  values are considerably higher than the static ones (0.58 and 0.51 for isolated and full-packed conditions, respectively) calculated at the CP optimized geometry, and also appreciably higher than the commonly used isotropic-model value 2/3. On the other

hand, CSORG1 experiences a CZ-PTZ distance shortening during the CPMD simulation with respect to its static configuration (average donor–acceptor distances of 11.42 and 11.70 Å in isolated and full-packed conditions versus the static values of 12.36 and 12.32 Å, respectively). These results suggest that both a static and an isotropic model should largely underestimate the FRET rate for CSORG1.

Turning now to CSORG4, in isolated conditions the CZ-PTZ distance goes through small variations during the first 7 ps of simulation, increases between 8 and 12 ps, markedly decreases around 13–14 ps and finally again increases in the last 7–6 ps. The simulation in full-packing conditions yields here large variations on  $r_{\text{DA}}$ , with a rapid increase during the first picoseconds (maximum of 13.80 Å at 6.35) and an overall zigzag-like decrease toward the minimum distance of 6.63 Å, recorded after 14.99 ps. It is worthwhile to notice that full-packing has on CSORG4 an opposite effect to that found in CSORG1, giving here rise to sizable oscillations and to a larger range of the sampled donor–acceptor distances with respect to that registered for the isolated simulation. At a first look, the evolution of  $\kappa^2$  in the isolated CSORG4 seems to closely follow the trend of the donor–acceptor distance: increasing within the first 13 ps of simulation, decreasing as  $r_{\text{DA}}$  decreases and strongly oscillating toward higher values in the last part of the simulation. The average value of 0.82 is considerably larger than that calculated on the CP optimized structure and closer to that of CSORG1, albeit its maximum value (2.99 reached at 17.44 ps) still remains lower than that calculated for CSORG1. Again, we note a considerable effect of the molecular packing on  $\kappa^2$ , with an increase in both the maximum (3.56, recorded at 19.35 ps, versus 2.99) and average (0.99 versus 0.82) values. More markedly than in CSORG1, a static picture is seen to provide  $\kappa^2$  values lower than the thermally averaged values both in isolated

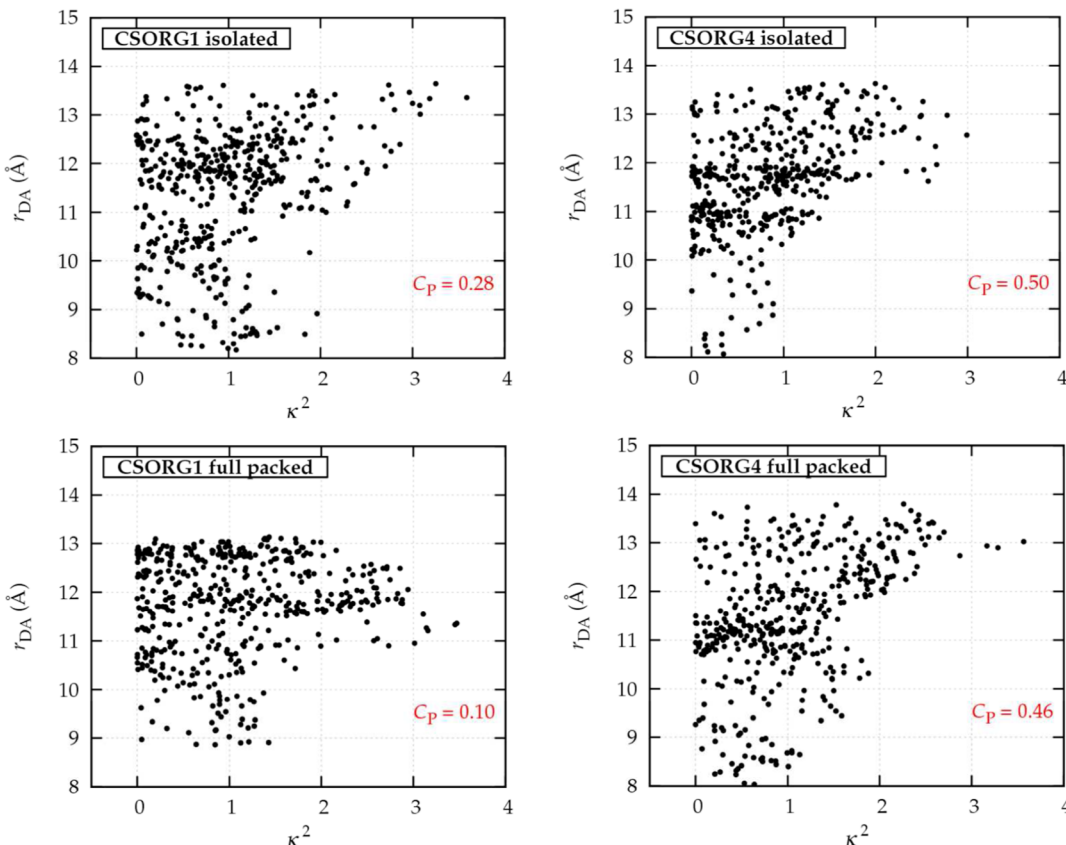


**Figure 4.** Scatter plots of  $r_{DA}$  versus  $\kappa^2$  for both CSORG1 (left panels) and CSORG4 (right panels) in isolated (top panels) and full-packed conditions (bottom panels). Each dot represents a single CPMD snapshot. Pearson's linear correlation coefficient ( $C_p$ ) between the two quantities is also reported.

and full-packed conditions (0.24 and 0.31 versus 0.82 and 0.99, respectively). These latter values are found to be, as in CSORG1, appreciably higher than the isotropic-model value 2/3. On the other hand, for CSORG4 the thermally averaged donor–acceptor distance varies only modestly with respect to the static picture both in isolated and full-packed conditions (11.41 and 11.17 Å versus 10.98 and 11.29 Å, respectively).

**3.2. Correlation between  $r_{DA}$  and  $\kappa^2$ .** As previously discussed, one of the key assumptions of the FRET model in the isotropic regime is the independence of  $\kappa^2$  and  $r_{DA}$ , allowing the determination of the donor–acceptor separation from FRET-rate measurements assuming an average  $\kappa^2$  of 2/3. If on the one hand, a number of combined MD simulations and FRET experiments on biological systems reported an overall agreement between the isotropic case and the MD calculated  $\kappa^2$ ,<sup>48,71,72</sup> for the present case, as discussed in ref 47, the molecular structure of the donor and acceptor moieties, their relative mobility and the flexibility of the linker chain may induce a degree of correlation between the two quantities.

Scatter plots of  $r_{DA}$  versus  $\kappa^2$  for both CSORG1 and CSORG4 in both isolated and full-packed conditions are shown in Figure 4. Pearson's linear correlation coefficients ( $C_p$ ) are also reported.

As is apparent from Figure 4, both dyes show correlation to a certain degree in both isolated and full-packed conditions. An interesting result emerging from the plots, and holding in both isolated and full-packed simulations, is that CSORG4 presents a relatively higher degree of correlation ( $C_p$  of 0.50/0.46 in isolated/full-packed conditions to be compared with 0.28/0.10 in CSORG1) between the relative orientation of CZ and PTZ

and their instantaneous distance. This suggests that the different molecular/electronic structure of the two dyes might translate into a different relative mobility of the CZ and PTZ subunits, when the acceptor is closer and more tightly bound to the anchoring group. In particular, the lower correlation in CSORG1 results from the higher rigidity of the PTZ moiety, which is electronically conjugated with the fixed –COOH group. In CSORG4, on the contrary, the rhodanine-3-acetic acid anchoring group (which, as mentioned is not conjugated with the PTZ acceptor unit) acts as a more flexible pivoting unit allowing for a prompter mutual response between the movements of the CZ and PTZ moieties. The extent of the relative mobility between the donor and acceptor units is also the key for rationalizing the lower correlation values in full-packed conditions. In fact, full-packed CSORG1 (standing up almost perpendicular to the TiO<sub>2</sub> surface) strongly feels the presence of the neighbor dyes and the related  $C_p$  falls down to 0.10 with respect to the isolated-conditions value of 0.28. On the other side, COSRG4 retains a higher degree of mobility due to a double-sized cell volume (see details in Section 2.2) with respect to CSORG1. Accordingly, the related  $C_p$  only shows a slight decrease in full-packed (0.46) versus isolated (0.50) conditions for CSORG4.

**3.3. FRET rate estimates.** We finally turn to a comparative analysis of the FRET rate estimates resulting from the three models considered so far: the static model, the isotropic model and the model including thermal fluctuations. Figure 5 displays the scaled FRET rates  $k'_F$  of both CSORG1 (left panels) and CSORG4 (right panels) in isolated (top panels) and full-packed conditions (bottom panels) as a function of time,

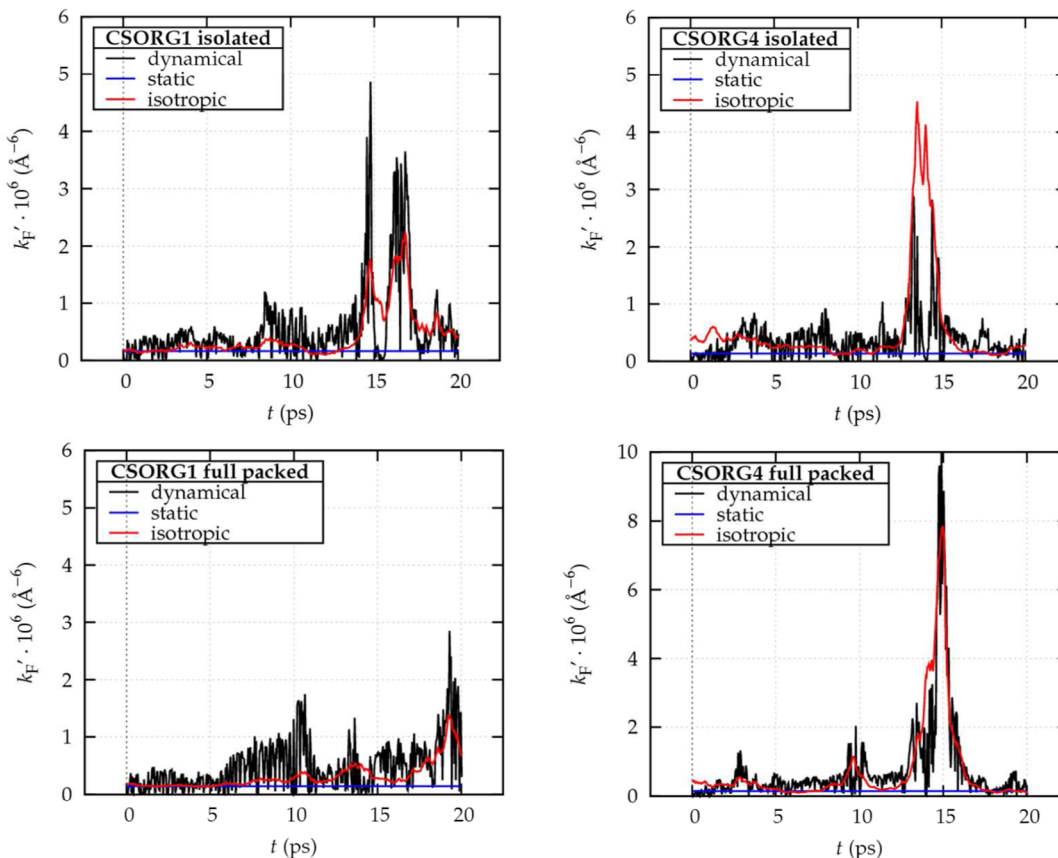


**Figure 5.** Scaled FRET rate  $k'_F$  (see eq 4) for both CSORG1 (left panels) and CSORG4 (right panels) in isolated (top panels) and full-packed conditions (bottom panels) computed using instantaneous values of  $\kappa^2$  (black line) or the isotropic-regime value  $2/3$  (red line). The scaled FRET rates given from the static  $\kappa^2$  and  $r_{\text{DA}}$  values are also reported (blue line).

computed using both the instantaneous values of  $\kappa^2$  (black line) and the isotropic-model value of  $2/3$  (red line). The scaled FRET rates given from the static (CP optimized)  $\kappa^2$  and  $r_{\text{DA}}$  values are also reported (blue line).

As previously suggested by the analysis of the FRET parameters in Section 3.1, the static FRET rates are largely exceeded both in the isotropic and thermally averaged picture. In the case of CSORG1, the isotropic model always yields a non-negligible underestimation of the FRET rates compared to the instantaneous values, which appears more pronounced in the last 10 ps of the simulation, where the orientational relaxation is faster and hence  $\kappa^2$  oscillations are stronger. Moving to the isolated CSORG4, the isotropic approximation is seen to predict largely overestimated  $k'_F$  in correspondence of the sizable donor–acceptor distance shortening, occurring here within 13 and 15 ps. Such distance decrease, in fact, is accompanied during the simulation by a simultaneous fall of  $\kappa^2$ , which is not accounted for in the isotropic regime. Interestingly, an opposite effect is encountered in full-packed conditions, where the isotropic-model estimate is lower than the fully dynamical one around 15 ps, when the CZ-PTZ distance strongly decreases. The close molecular packing seems, in fact, to promote, in this region (between 13 and 15 ps), a favorable orientation between the transition dipole moments of the CZ and PTZ moieties, resulting in highly enhanced energy transfer rates.

The above outlined picture is fully confirmed by the scaled FRET rate time-averaged values. Average values of  $k'_F$  for both isolated and full-packed CSORG1 and CSORG4 computed in

both the isotropic and thermally averaged regime are reported in Table 2 together with the values obtained in the static picture. In line with the above discussion following the analysis of Figure 5, the predicted FRET rates in a static picture are in any case considerably lower than the average values obtained both in the isotropic and fully dynamical models. On the other hand, with the exception of full-packed CSORG4, also the average rates estimated using the instantaneous distances and an average  $2/3$  value for  $\kappa^2$  (isotropic model) for the remaining three cases are a poor approximation to those calculated with the instantaneous values of  $\kappa^2$ . In the isotropic approximation, in fact, the FRET rate of CSORG1 is underestimated of 25% and 51% in isolated and full-packed conditions, respectively. For CSORG4, on the contrary, a large overestimation (40%) is found in the isolated-condition simulation, while a surprisingly good agreement, within 3%, is obtained in full-packed conditions.

In Table 2, the thermally averaged rates for intermolecular FRET processes occurring (see section 2.3) in full-packed conditions are also provided. As is evident, the predicted intermolecular  $k'_F$  values are always negligible (from 1 to 2 order of magnitude lower) with respect to those calculated for the intramolecular energy transfer, CZ(0,0)-PTZ(0,0). This indicates that even in full-packed conditions the distance between the CZ and the PTZ moieties lying on adjacent molecules is too long to allow a competitive intermolecular FRET.

**Table 2. Static (CP-Optimized), Isotropic, and Fully Dynamical Average Values of the Scaled FRET Rate  $k'_F$  for CSORG1 and CSORG4 under both Isolated and Full-Packed Conditions<sup>a</sup>**

		static	isotropic	thermally averaged
CSORG1				
isolated				
$k'_F \times 10^6 (\text{\AA}^{-6})$		0.163	0.436	0.573
full-packed				
$k'_F \times 10^6 (\text{\AA}^{-6})$	CZ(0,0)-PTZ(0,0)	0.146	0.315	0.477
	CZ(0,0)-PTZ(1,0)			0.085
	CZ(1,0)-PTZ(0,0)			0.004
	CZ(0,0)-PTZ(0,1)			0.042
	CZ(0,1)-PTZ(0,0)			0.034
CSORG4				
isolated				
$k'_F \times 10^6 (\text{\AA}^{-6})$		0.135	0.530	0.379
full-packed				
$k'_F \times 10^6 (\text{\AA}^{-6})$	CZ(0,0)-PTZ(0,0)	0.151	0.750	0.769
	CZ(0,0)-PTZ(1,0)			0.031
	CZ(1,0)-PTZ(0,0)			0.041
	CZ(0,0)-PTZ(0,1)			0.041
	CZ(0,1)-PTZ(0,0)			0.036

<sup>a</sup>Estimates of intermolecular scaled FRET rates (see section 2.3) are also given.

## 4. CONCLUSIONS

In this work, a dynamical modeling of Förster resonance energy transfer (FRET) processes in  $\text{TiO}_2$ -adsorbed dyadic dye systems was addressed for the first time within a combined Car-Parrinello molecular dynamics (CPMD) and TDDFT framework. Two dyadic carbazole- (CZ-) phenothiazine (PTZ) dyes were considered, where the CZ unit, linked to PTZ via an alkyl  $\text{C}_6\text{H}_{12}$  chain, acts as an antenna donor and the PTZ unit is a  $\text{TiO}_2$ -anchored acceptor. The considered dyes, termed CSORG1 and CSORG4 and differing for the anchoring group affecting the relative mobility of the CZ and PTZ units, were modeled both in isolated and full-packed adsorption conditions, where intermolecular processes can also occur. We monitored along the CPMD trajectories the geometrical parameters (relative donor–acceptor distance  $r_{\text{DA}}$  and relative orientation  $\kappa^2$  between the donor and acceptor transition dipole moments) concurring in determining the FRET rate and analyzed the results in relation to a static and a so-called isotropic model whereby donor and acceptor moieties are allowed to rapidly sample all possible orientations and no correlation between the donor/acceptor distance and orientation is implied.

A first result emerging from our simulations is that for both dyes a static (minimum-energy) picture provides largely underestimated FRET rates in both isolated and full-packed conditions when compared to the dynamically averaged one. The isotropic model, on the other hand, though significantly improving over the static one, still fails to reproduce the dynamically averaged values in three out of the four considered cases. This indicates that accounting for thermal fluctuations should be mandatory for a proper modeling of FRET processes in dyadic dye– $\text{TiO}_2$  DSSCs as those modeled in our study.

Moreover, assuming, as one implicitly does in adopting the isotropic approximation, that the donor–acceptor distance  $r_{\text{DA}}$  and orientation factor  $\kappa^2$  are uncorrelated is found not to be

justified in all of the considered tests. For both dyes, in fact, a certain degree of correlation is found between  $r_{\text{DA}}$  and  $\kappa^2$  in both isolated and full-packed conditions, the extent of which is deemed to depend on the structural differences of the dyes and on the degree of donor/acceptor mobility allowed by the adsorption conditions.

A final outcome of our simulations is that intermolecular FRET processes, which are likely to occur in full-packed conditions, are found to be of negligible importance (1 or 2 orders of magnitude slower) as compared to intramolecular ones for both the considered dyes.

## ■ AUTHOR INFORMATION

### Corresponding Authors

\* (S.R.) E-mail: srampino@thch.unipg.it.

\* (M.P.) E-mail: chiara@thch.unipg.it.

\* (F.D.A.) E-mail: filippo@thch.unipg.it.

### Notes

The authors declare no competing financial interest.

## ■ ACKNOWLEDGMENTS

R.A.-P. and R.AU.-L. have been supported by the Grants Fondecyt No. 1150629, Millennium Nucleus RC120001, Conicyt No. 21110486, UNAB-DI-420-13/I, and AKA-Finland-Conicyt-Chile. M.P., S.R., E.M., and F.D.A. thank the CNR-EFOR for partial financial support.

## ■ REFERENCES

- (1) Kim, H.-S.; Lee, C.-R.; Im, J.-H.; Lee, K.-B.; Moehl, T.; Marchioro, A.; Moon, S.-J.; Humphry-Baker, R.; Yum, J.-H.; Moser, J. E. Lead Iodide Perovskite Sensitized All-Solid-State Submicron Thin Film Mesoscopic Solar Cell with Efficiency Exceeding 9%. *Sci. Rep.* **2012**, *2*, 591 DOI: 10.1038/srep00591.
- (2) De Angelis, F. Modeling Materials and Processes in Hybrid/Organic Photovoltaics: From Dye-Sensitized to Perovskite Solar Cells. *Acc. Chem. Res.* **2014**, *47*, 3349–3360.
- (3) O'Regan, B.; Grätzel, M. A Low-Cost, High-Efficiency Solar Cell Based on Dye-Sensitized Colloidal  $\text{Tio}_2$  Films. *Nature* **1991**, *353*, 737–740.
- (4) Grätzel, M. Recent Advances in Sensitized Mesoscopic Solar Cells. *Acc. Chem. Res.* **2009**, *42*, 1788–1798.
- (5) Hagfeldt, A.; Grätzel, M. Light-Induced Redox Reactions in Nanocrystalline Systems. *Chem. Rev.* **1995**, *95*, 49–68.
- (6) Mathew, S.; Yella, A.; Gao, P.; Humphry-Baker, R.; Basile, F. E. C.; Ashari-Astani, N.; Tavernelli, I.; Rothlisberger, U.; NazeeruddinMd, K.; Grätzel, M. Dye-Sensitized Solar Cells with 13% Efficiency Achieved through the Molecular Engineering of Porphyrin Sensitizers. *Nat. Chem.* **2014**, *6*, 242–247.
- (7) Boschloo, G.; Hagfeldt, A. Characteristics of the Iodide/Triiodide Redox Mediator in Dye-Sensitized Solar Cells. *Acc. Chem. Res.* **2009**, *42*, 1819–1826.
- (8) Nazeeruddin, M. K.; Pechy, P.; Grätzel, M. Efficient Panchromatic Sensitization of Nanocrystalline  $\text{TiO}_2$  Films by a Black Dye Based on a Trithiocyanato-Ruthenium Complex. *Chem. Commun.* **1997**, *0*, 1705–1706.
- (9) Nazeeruddin, M. K.; Kay, A.; Rodicio, I.; Humphry-Baker, R.; Mueller, E.; Liska, P.; Vlachopoulos, N.; Grätzel, M. Conversion of Light to Electricity by Cis-X2bis(2,2'-Bipyridyl-4,4'-Dicarboxylate)-Ruthenium(II) Charge-Transfer Sensitizers (X = Cl-, Br-, I-, CN-, and SCN-) on Nanocrystalline Titanium Dioxide Electrodes. *J. Am. Chem. Soc.* **1993**, *115*, 6382–6390.
- (10) Nazeeruddin, M. K.; Zakeeruddin, S. M.; Humphry-Baker, R.; Jirousek, M.; Liska, P.; Vlachopoulos, N.; Shklover, V.; Fischer, C.-H.; Grätzel, M. Acid-Base Equilibria of (2,2'-Bipyridyl-4,4'-Dicarboxylic Acid)Ruthenium(II) Complexes and the Effect of Protonation on

- Charge-Transfer Sensitization of Nanocrystalline Titania. *Inorg. Chem.* **1999**, *38*, 6298–6305.
- (11) Nazeeruddin, M. K.; Pechy, P.; Renouard, T.; Zakeeruddin, S. M.; Humphry-Baker, R.; Comte, P.; Liska, P.; Cevey, L.; Costa, E.; Shklover, V.; et al. Engineering of Efficient Panchromatic Sensitzers for Nanocrystalline TiO<sub>2</sub>-Based Solar Cells. *J. Am. Chem. Soc.* **2001**, *123*, 1613–1624.
  - (12) Mishra, A.; Fischer, M. K. R.; Bäuerle, P. Metal-Free Organic Dyes for Dye-Sensitized Solar Cells: From Structure: Property Relationships to Design Rules. *Angew. Chem., Int. Ed.* **2009**, *48*, 2474–2499.
  - (13) Chandrasekharan, M.; Chiranjeevi, B.; Gupta, K. S. V.; Singh, S. P.; Islam, A.; Han, L.; Kantam, M. L. Simple Metal-Free Organic D-II-A Dyes with Alkoxy- or Fluorine Substitutions: Application in Dye Sensitized Solar Cells. *J. Nanosci. Nanotechnol.* **2012**, *12*, 4489–4494.
  - (14) Lee, C.-P.; Lin, R. Y.-Y.; Lin, L.-Y.; Li, C.-T.; Chu, T.-C.; Sun, S.-S.; Lin, J. T.; Ho, K.-C. Recent Progress in Organic Sensitzers for Dye-Sensitized Solar Cells. *RSC Adv.* **2015**, *5*, 23810–23825.
  - (15) Ito, S.; Miura, H.; Uchida, S.; Takata, M.; Sumioka, K.; Liska, P.; Comte, P.; Pechy, P.; Grätzel, M. High-Conversion-Efficiency Organic Dye-Sensitized Solar Cells with a Novel Indoline Dye. *Chem. Commun.* **2008**, 5194–5196.
  - (16) Zeng, W.; Cao, Y.; Bai, Y.; Wang, Y.; Shi, Y.; Zhang, M.; Wang, F.; Pan, C.; Wang, P. Efficient Dye-Sensitized Solar Cells with an Organic Photosensitizer Featuring Orderly Conjugated Ethylenedioxothiophene and Dithienosilole Blocks. *Chem. Mater.* **2010**, *22*, 1915–1925.
  - (17) Zhang, M.; Wang, Y.; Xu, M.; Ma, W.; Li, R.; Wang, P. Design of High-Efficiency Organic Dyes for Titania Solar Cells Based on the Chromophoric Core of Cyclopentadithiophene-Benzothiadiazole. *Energy Environ. Sci.* **2013**, *6*, 2944–2949.
  - (18) Kakiage, K.; Aoyama, Y.; Yano, T.; Otsuka, T.; Kyomen, T.; Unno, M.; Hanaya, M. An Achievement of over 12% Efficiency in an Organic Dye-Sensitized Solar Cell. *Chem. Commun.* **2014**, *50*, 6379–6381.
  - (19) Yao, Z.; Zhang, M.; Wu, H.; Yang, L.; Li, R.; Wang, P. Donor/Acceptor Indenoperylene Dye for Highly Efficient Organic Dye-Sensitized Solar Cells. *J. Am. Chem. Soc.* **2015**, *137*, 3799–3802.
  - (20) Yella, A.; Lee, H.-W.; Tsao, H. N.; Yi, C.; Chandiran, A. K.; Nazeeruddin, M. K.; Diau, E. W.-G.; Yeh, C.-Y.; Zakeeruddin, S. M.; Grätzel, M. Porphyrin-Sensitized Solar Cells with Cobalt (Ii/Iii)-Based Redox Electrolyte Exceed 12% Efficiency. *Science* **2011**, *334*, 629–634.
  - (21) Clifford, J. N.; Forneli, A.; Chen, H.; Torres, T.; Tan, S.; Palomares, E. Co-Sensitized Dscs: Dye Selection Criteria for Optimized Device Voc and Efficiency. *J. Mater. Chem.* **2011**, *21*, 1693–1696.
  - (22) Sayama, K.; Tsukagoshi, S.; Mori, T.; Hara, K.; Ohga, Y.; Shinpou, A.; Abe, Y.; Suga, S.; Arakawa, H. Efficient Sensitization of Nanocrystalline TiO<sub>2</sub> Films with Cyanine and Merocyanine Organic Dyes. *Sol. Energy Mater. Sol. Cells* **2003**, *80*, 47–71.
  - (23) Martínez-Díaz, M. V.; de la Torre, G.; Torres, T. Lighting Porphyrins and Phthalocyanines for Molecular Photovoltaics. *Chem. Commun.* **2010**, *46*, 7090–7108.
  - (24) Chen, Y.; Zeng, Z.; Li, C.; Wang, W.; Wang, X.; Zhang, B. Highly Efficient Co-Sensitization of Nanocrystalline TiO<sub>2</sub> Electrodes with Plural Organic Dyes. *New J. Chem.* **2005**, *29*, 773–776.
  - (25) Yum, J.-H.; Jang, S.-R.; Walter, P.; Geiger, T.; Nüesch, F.; Kim, S.; Ko, J.; Grätzel, M.; Nazeeruddin, M. K. Efficient Co-Sensitization of Nanocrystalline TiO<sub>2</sub> Films by Organic Sensitzers. *Chem. Commun.* **2007**, 4680–4682.
  - (26) Lan, C.-M.; Wu, H.-P.; Pan, T.-Y.; Chang, C.-W.; Chao, W.-S.; Chen, C.-T.; Wang, C.-L.; Lin, C.-Y.; Diau, E. W.-G. Enhanced Photovoltaic Performance with Co-Sensitization of Porphyrin and an Organic Dye in Dye-Sensitized Solar Cells. *Energy Environ. Sci.* **2012**, *5*, 6460–6464.
  - (27) Yum, J.-H.; Baranoff, E.; Wenger, S.; Nazeeruddin, M. K.; Grätzel, M. Panchromatic Engineering for Dye-Sensitized Solar Cells. *Energy Environ. Sci.* **2011**, *4*, 842–857.
  - (28) Campbell, W. M.; Burrell, A. K.; Officer, D. L.; Jolley, K. W. Porphyrins as Light Harvesters in the Dye-Sensitised TiO<sub>2</sub> Solar Cell. *Coord. Chem. Rev.* **2004**, *248*, 1363–1379.
  - (29) Warnan, J.; Pellegrin, Y.; Blart, E.; Odobel, F. Supramolecular Light Harvesting Antennas to Enhance Absorption Cross-Section in Dye-Sensitized Solar Cells. *Chem. Commun.* **2012**, *48*, 675–677.
  - (30) Warnan, J.; Buchet, F.; Pellegrin, Y.; Blart, E.; Odobel, F. Panchromatic Trichromophoric Sensitizer for Dye-Sensitized Solar Cells Using Antenna Effect. *Org. Lett.* **2011**, *13*, 3944–3947.
  - (31) Zhao, L.; Wagner, P.; Elliott, A. B. S.; Griffith, M. J.; Clarke, T. M.; Gordon, K. C.; Mori, S.; Mozer, A. J. Enhanced Performance of Dye-Sensitized Solar Cells Using Carbazole-Substituted Di-Chromophoric Porphyrin Dyes. *J. Mater. Chem. A* **2014**, *2*, 16963–16977.
  - (32) Kuroda, Y.; Sugou, K.; Sasaki, K. Nonamer Porphyrin Assembly: Antenna Effect on Energy Transfer. *J. Am. Chem. Soc.* **2000**, *122*, 7833–7834.
  - (33) Serin, J. M.; Brousmiche, D. W.; Fréchet, J. M. J. A Fret-Based Ultraviolet to Near-Infrared Frequency Converter. *J. Am. Chem. Soc.* **2002**, *124*, 11848–11849.
  - (34) Förster, T. 10th Spiers Memorial Lecture. Transfer Mechanisms of Electronic Excitation. *Discuss. Faraday Soc.* **1959**, *27*, 7–17.
  - (35) Odobel, F.; Pellegrin, Y.; Warnan, J. Bio-Inspired Artificial Light-Harvesting Antennas for Enhancement of Solar Energy Capture in Dye-Sensitized Solar Cells. *Energy Environ. Sci.* **2013**, *6*, 2041–2052.
  - (36) Mårtensson, J. Calculation of the Förster Orientation Factor for Donor-Acceptor Systems with One Chromophore of Threefold or Higher Symmetry: Zinc Porphyrin. *Chem. Phys. Lett.* **1994**, *229*, 449–456.
  - (37) Clegg, R. M. [18] Fluorescence Resonance Energy Transfer and Nucleic Acids. In *Methods in Enzymology*; David, M. J., Lilley, J. E. D., Eds. Academic Press: San Diego, CA, 1992; Vol. 211, pp 353–388.
  - (38) Lilley, D. M. J.; Wilson, T. J. Fluorescence Resonance Energy Transfer as a Structural Tool for Nucleic Acids. *Curr. Opin. Chem. Biol.* **2000**, *4*, 507–517.
  - (39) Deniz, A. A.; Laurence, T. A.; Dahan, M.; Chemla, D. S.; Schultz, P. G.; Weiss, S. Ratiometric Single-Molecule Studies of Freely Diffusing Biomolecules. *Annu. Rev. Phys. Chem.* **2001**, *52*, 233–253.
  - (40) Ha, T. Single-Molecule Fluorescence Resonance Energy Transfer. *Methods* **2001**, *25*, 78–86.
  - (41) Barkai, E.; Jung, Y.; Silbey, R. Theory of Single-Molecule Spectroscopy: Beyond the Ensemble Average. *Annu. Rev. Phys. Chem.* **2004**, *55*, 457–507.
  - (42) Johnson, C.; Slaughter, B.; Unruh, J.; Price, E. S. Fluorescence Probes of Protein Dynamics and Conformations in Freely Diffusing Molecules. In *Reviews in Fluorescence 2006*; Geddes, C., Lakowicz, J., Eds.; Springer: Berlin, 2006; Vol. 2006, pp 239–259.
  - (43) Scholes, G. D. Long-Range Resonance Energy Transfer in Molecular Systems. *Annu. Rev. Phys. Chem.* **2003**, *54*, 57–87.
  - (44) Muñoz-Losa, A.; Curutchet, C.; Krueger, B. P.; Hartsell, L. R.; Mennucci, B. Fretting About Fret: Failure of the Ideal Dipole Approximation. *Biophys. J.* **2009**, *96*, 4779–4788.
  - (45) Speelman, A. L.; Muñoz-Losa, A.; Hinkle, K. L.; VanBeek, D. B.; Mennucci, B.; Krueger, B. P. Using Molecular Dynamics and Quantum Mechanics Calculations to Model Fluorescence Observables. *J. Phys. Chem. A* **2011**, *115*, 3997–4008.
  - (46) Hsu, C.-P.; You, Z.-Q.; Chen, H.-C. Characterization of the Short-Range Couplings in Excitation Energy Transfer. *J. Phys. Chem. C* **2008**, *112*, 1204–1212.
  - (47) VanBeek, D. B.; Zwier, M. C.; Shorb, J. M.; Krueger, B. P. Fretting About Fret: Correlation between K and R. *Biophys. J.* **2007**, *92*, 4168–4178.
  - (48) Beierlein, F. R.; Othersen, O. G.; Lanig, H.; Schneider, S.; Clark, T. Simulating Fret from Tryptophan: Is the Rotamer Model Correct? *J. Am. Chem. Soc.* **2006**, *128*, 5142–5152.
  - (49) Merchant, K. A.; Best, R. B.; Louis, J. M.; Gopich, I. V.; Eaton, W. A. Characterizing the Unfolded States of Proteins Using Single-Molecule Fret Spectroscopy and Molecular Simulations. *Proc. Natl. Acad. Sci. U. S. A.* **2007**, *104*, 1528–1533.

- (50) Schuler, B.; Lipman, E. A.; Eaton, W. A. Probing the Free-Energy Surface for Protein Folding with Single-Molecule Fluorescence Spectroscopy. *Nature* **2002**, *419*, 743–747.
- (51) Margittai, M.; Widengren, J.; Schweinberger, E.; Schröder, G. F.; Felekyan, S.; Haustein, E.; König, M.; Fasshauer, D.; Grubmüller, H.; Jahn, R.; et al. Single-Molecule Fluorescence Resonance Energy Transfer Reveals a Dynamic Equilibrium between Closed and Open Conformations of Syntaxin 1. *Proc. Natl. Acad. Sci. U. S. A.* **2003**, *100*, 15516–15521.
- (52) Unruh, J. R.; Kuczera, K.; Johnson, C. K. Conformational Heterogeneity of a Leucine Enkephalin Analogue in Aqueous Solution and Sodium Dodecyl Sulfate Micelles: Comparison of Time-Resolved Fret and Molecular Dynamics Simulations. *J. Phys. Chem. B* **2009**, *113*, 14381–14392.
- (53) Hoefling, M.; Lima, N.; Haenni, D.; Seidel, C. A. M.; Schuler, B.; Grubmüller, H. Structural Heterogeneity and Quantitative Fret Efficiency Distributions of Polyprolines through a Hybrid Atomistic Simulation and Monte Carlo Approach. *PLoS One* **2011**, *6*, e19791.
- (54) Pastore, M.; De Angelis, F. Intermolecular Interactions in Dye-Sensitized Solar Cells: A Computational Modeling Perspective. *J. Phys. Chem. Lett.* **2013**, *4*, 956–974.
- (55) Pastore, M.; De Angelis, F. First-Principles Computational Modeling of Fluorescence Resonance Energy Transfer in Co-Sensitized Dye Solar Cells. *J. Phys. Chem. Lett.* **2012**, *3*, 2146–2153.
- (56) Marotta, G.; Reddy, M. A.; Singh, S. P.; Islam, A.; Han, L.; De Angelis, F.; Pastore, M.; Chandrasekharan, M. Novel Carbazole-Phenothiazine Dyads for Dye-Sensitized Solar Cells: A Combined Experimental and Theoretical Study. *ACS Appl. Mater. Interfaces* **2013**, *5*, 9635–9647.
- (57) Hoke, E. T.; Hardin, B. E.; McGehee, M. D. Modeling the Efficiency of Förster Resonant Energy Transfer from Energy Relay Dyes in Dye-Sensitized Solar Cells. *Opt. Express* **2010**, *18*, 3893–3904.
- (58) Aragó, J.; Troisi, A. Dynamics of the Excitonic Coupling in Organic Crystals. *Phys. Rev. Lett.* **2015**, *114*, 026402.
- (59) Stangl, T.; Wilhelm, P.; Schmitz, D.; Remmerssen, K.; Henzel, S.; Jester, S.-S.; Höger, S.; Vogelsang, J.; Lupton, J. M. Temporal Fluctuations in Excimer-Like Interactions between π-Conjugated Chromophores. *J. Phys. Chem. Lett.* **2015**, *6*, 1321–1326.
- (60) Renaud, N.; Grozema, F. C. Intermolecular Vibrational Modes Speed up Singlet Fission in Perylenediimide Crystals. *J. Phys. Chem. Lett.* **2015**, *6*, 360–365.
- (61) Förster, T. Zwischenmolekulare Energiewanderung Und Fluoreszenz. *Ann. Phys.* **1948**, *437*, 55–75.
- (62) Pastore, M.; De Angelis, F. Computational Modelling of TiO<sub>2</sub> Surfaces Sensitized by Organic Dyes with Different Anchoring Groups: Adsorption Modes, Electronic Structure and Implication for Electron Injection/Recombination. *Phys. Chem. Chem. Phys.* **2012**, *14*, 920–928.
- (63) Frisch, M. J.; Trucks, G. W.; Schlegel, H. B.; Scuseria, G. E.; Robb, M. A.; Cheeseman, J. R.; Scalmani, G.; Barone, V.; Mennucci, B.; Petersson, G. A., et al. *Gaussian 09*, Revision A.1; Gaussian, Inc.: Wallingford, CT, 2009.
- (64) Lynch, B. J.; Fast, P. L.; Harris, M.; Truhlar, D. G. Adiabatic Connection for Kinetics. *J. Phys. Chem. A* **2000**, *104*, 4811.
- (65) Cossi, M.; Rega, N.; Scalmani, G.; Barone, V. Energies, Structures, and Electronic Properties of Molecules in Solution with the C-PCM Solvation Model. *J. Comput. Chem.* **2003**, *24*, 669–681.
- (66) Car, R.; Parrinello, M. Unified Approach for Molecular Dynamics and Density-Functional Theory. *Phys. Rev. Lett.* **1985**, *55*, 2471–2474.
- (67) Giannozzi, P.; Baroni, S.; Bonini, N.; Calandra, M.; Car, R.; Cavazzoni, C.; Ceresoli, D.; Chiarotti, G. L.; Cococcioni, M.; Dabo, I. Quantum Espresso: A Modular and Open-Source Software Project for Quantum Simulations of Materials. *J. Phys.: Condens. Matter* **2009**, *21*, 395502.
- (68) Becke, A. D. Density-Functional Exchange-Energy Approximation with Correct Asymptotic Behaviour. *Phys. Rev. A: At., Mol., Opt. Phys.* **1988**, *38*, 3098–3100.
- (69) Lee, C.; Yang, W.; Parr, R. G. Development of the Colle-Salvetti Correlation-Energy Formula into a Functional of the Electron Density. *Phys. Rev. B: Condens. Matter Mater. Phys.* **1988**, *37*, 785–789.
- (70) Giannozzi, P.; De Angelis, F.; Car, R. First-Principle Molecular Dynamics with Ultrasoft Pseudopotentials: Parallel Implementation and Application to Extended Bioinorganic Systems. *J. Chem. Phys.* **2004**, *120*, 5903–5915.
- (71) Jean, J. M.; Krueger, B. P. Structural Fluctuations and Excitation Transfer between Adenine and 2-Aminopurine in Single-Stranded Deoxytrinucleotides. *J. Phys. Chem. B* **2006**, *110*, 2899–2909.
- (72) Srinivas, G.; Bagchi, B. Effect of Orientational Motion of Mobile Chromophores on the Dynamics of Förster Energy Transfer in Polymers. *J. Phys. Chem. B* **2001**, *105*, 9370–9374.